biology

MDPI

Article

Aerobic Exercise Ameliorates Type 2 Diabetic Nephropathy and Correlates with EPHX1 and Attenuated Renal Ferroptosis in Mice

Qin Ru [1,†], Xiao Xiang [1,†], Bei Cheng [1], Congyue Xu [1], Lin Chen [1] and Yuxiang Wu [1,2,*]

[1] Institute of Intelligent Sport and Proactive Health, Department of Health and Physical Education, Jianghan University, Wuhan 430056, China; ruqin@jhun.edu.cn (Q.R.); m13403047529@163.com (X.X.); chengbei08@163.com (B.C.); xucy@jhun.edu.cn (C.X.); lchen@jhun.edu.cn (L.C.)

[2] Wuhan (China-Cuba) Belt and Road Joint Laboratory on Natural Products, Jianghan University, Wuhan 430056, China

* Correspondence: yxwu@jhun.edu.cn; Tel.: +86-15802755474

† These authors contribute equally to this work.

Simple Summary

Diabetic nephropathy is a common complication of type 2 diabetes and can lead to kidney failure. Aerobic exercise is a safe non-drug therapy for diabetes, but how different-intensity exercise protects the kidney remains unclear. In this study, we found that aerobic exercise alleviated diabetic nephropathy partly by reducing ferroptosis-associated molecular alterations in renal tissue. Higher-intensity exercise produced more obvious protective effects. We also identified that the molecule EPHX1 and arachidonic-acid metabolism may participate in this protective process. This work offers experimental evidence supporting exercise as an intervention strategy against diabetic nephropathy.

Abstract

Objectives: Diabetic nephropathy is a major microvascular complication of type 2 diabetes and a leading cause of end-stage renal disease worldwide. Ferroptosis, an iron-dependent regulated cell death, participates in renal tissue injury under diabetic conditions. Aerobic exercise serves as a safe non-pharmacological intervention for diabetes, yet how different-intensity aerobic exercise modulates renal ferroptosis in diabetic nephropathy remains poorly defined. This study aimed to explore the protective effects and underlying mechanisms of aerobic exercise against diabetic nephropathy. **Methods:** A type 2 diabetic nephropathy mouse model was established by high-fat-diet feeding combined with multiple low-dose streptozotocin injections. Mice received 8-week treadmill-based interventions, including low-intensity (LA), moderate-intensity (MA), high-intensity aerobic exercise (HA), and high-intensity interval training (HIIT). Metabolic phenotypes, renal function, histopathological lesions, iron homeostasis, oxidative stress and ferroptosis-related protein expression were detected. **Results:** All four exercise regimens alleviated hyperglycemia and insulin resistance, improved renal function, mitigated glomerular-tubular damage and renal fibrosis. Mechanistically, aerobic exercise restored renal iron homeostasis, elevated renal and serum GSH levels, and reduced renal and serum MDA content. HA and HIIT significantly upregulated GPX4 and downregulated ACSL4, SLC39A14 and FTH; partial significant changes were observed in LA and MA groups, thus attenuating molecular features associated with renal ferroptosis. Further bioinformatic screening combined with in vivo validation identified EPHX1 as a potential associated candidate molecule, whose related arachidonic-acid metabolism may correlate with exercise-driven modulation of these ferroptosis-related molecular alterations. LA and MA groups exhibited a decreasing trend in renal EPHX1 expression and arachidonic-acid level without statistical significance, while HA and HIIT groups showed significant reductions. **Conclusions:** Appropriate

Check for updates

Academic Editor: Kenneth N. White

Received: 16 September 2026
Revised: 20 October 2026
Accepted: 28 October 2026
Published: 18 November 2026

Copyright: © 2026 by the authors. Licensee MDPI, Basel, Switzerland. This article is an open access article distributed under the terms and conditions of the Creative Commons Attribution (CC BY) license.

aerobic exercise ameliorates diabetic nephropathy and attenuates molecular signatures associated with renal ferroptosis. EPHX1-dependent arachidonic-acid metabolism represents a potential correlative molecular mechanism for exercise-mediated renoprotection. This study provides experimental evidence and mechanistic reference for non-pharmacological intervention of diabetic nephropathy.

Keywords: diabetic nephropathy; aerobic exercise; ferroptosis; EPHX1; arachidonic-acid metabolism

1. Introduction

Diabetes mellitus has become a global public health crisis with rapidly increasing morbidity due to population aging and lifestyle changes [1]. Diabetic nephropathy, one of the most common microvascular complications of diabetes, is the leading cause of end-stage renal disease globally [2]. Long-term persistent hyperglycemia induces typical pathological changes in the kidney, including glomerular basement-membrane thickening, mesangial hyperplasia, tubular interstitial fibrosis, and progressive renal dysfunction, severely threatening patients' life quality and survival rate [3,4]. Current clinical management mainly focuses on symptomatic control of blood glucose and blood pressure to slow disease progression. However, many patients still progress toward end-stage renal disease, because existing therapies lack targeted strategies against core pathogenic renal cell-death pathways [5–7]. Growing evidence highlights ferroptosis as a critical driver of renal parenchymal injury in diabetic nephropathy. Dysregulated iron homeostasis and excessive lipid peroxidation triggered by the diabetic microenvironment can initiate ferroptotic signaling in glomerular podocytes and renal tubular epithelial cells, promoting tissue destruction and accelerating diabetic nephropathy progression [8–10]. Nevertheless, the key regulatory targets linking metabolic disorders and renal ferroptosis in diabetic nephropathy have not been fully clarified, and safe and precise non-pharmacological intervention means and their underlying systematic molecular mechanisms remain to be further explored and supplemented.

Ferroptosis is an iron-dependent novel programmed cell death, distinct from apoptosis, pyroptosis and autophagy, which is characterized by intracellular iron overload and excessive lipid peroxidation accumulation [11–13]. Excessive iron deposition in renal tissues triggers the Fenton reaction, promotes excessive reactive oxygen species (ROS) generation [14], aggravates lipid peroxidation damage, and ultimately induces renal intrinsic cell death, accelerating renal structural and functional deterioration [15,16]. Multiple lines of pre-clinical work have confirmed that suppression of ferroptosis can mitigate experimental diabetic nephropathy; yet, key regulatory molecules bridging metabolic stress and renal ferroptosis are still insufficiently characterized.

Arachidonic acid is a pivotal polyunsaturated fatty acid substrate whose metabolites serve as precursors for lipid peroxidation that executes ferroptosis [17,18]. Cytochrome P450 epoxygenases convert arachidonic acid into four regioisomers of epoxyeicosatrienoic acids (EETs), bioactive epoxy-fatty acids with anti-oxidative and cytoprotective properties [19,20]. Two epoxide hydrolases mediate EET hydrolysis: microsomal epoxide hydrolase 1 (EPHX1) and soluble epoxide hydrolase 2 (EPHX2) [21]. EPHX2 is the canonical cytosolic enzyme considered responsible for the majority of renal EET catabolisms under in vitro conditions. However, renal EPHX1 is expressed in proximal/distal tubules and glomerular endothelial cells, and in vivo evidence from kidney models demonstrates that EPHX1 also participates in EET hydrolysis, converting arachidonic-acid-derived EETs into less biologically active dihydroxyeicosatrienoic acids (DHETs) and remodeling renal arachidonic-acid oxylipin pools [22,23]. Distinct from EPHX2, EPHX1 also catalyzes

the hydrolysis of 2-arachidonoylglycerol to liberate free arachidonic acid [24]. Elevated intracellular arachidonic acid promotes the formation of arachidonic-acid-containing phosphatidylethanolamine, a lipid species highly prone to oxidative modification upon iron overload and ROS accumulation. This process requires arachidonic acid to be incorporated into membrane phospholipids via acyl-CoA synthetase long-chain family member 4 (ACSL4) and lysophosphatidylcholine acyltransferase 3 (LPCAT3) to generate peroxidizable lipid substrates that initiate and drive ferroptosis [25,26]. Accumulating evidence links EPHX1 to fatty acid metabolism and ferroptosis [24], yet the functional involvement of the EPHX1-arachidonic-acid signaling axis in diabetic nephropathy-associated ferroptosis has not been documented.

Aerobic exercise is a safe, economical intervention for diabetes and its complications [27]. Existing studies have verified that aerobic exercise can improve insulin resistance [28,29], reduce blood glucose levels, alleviate renal oxidative stress and inflammatory damage, and effectively delay diabetic nephropathy progression [30,31]. Aerobic exercise elicits sustained systemic and local metabolic adaptations, reinforces endogenous antioxidant defense capacity and remodels iron homeostasis networks [32,33]. These persistent physiological adaptations create a biological basis by which chronic exercise may restrain ferroptosis-driven renal injury and preserve kidney health. Nevertheless, most current studies only confirm the protective effect of exercise on diabetic nephropathy, lacking systematic exploration of the correlation between exercise intervention and renal ferroptosis. Moreover, the differences in therapeutic effects of different intensities of aerobic exercise on diabetic nephropathy and the optimal exercise intensity for inhibiting renal ferroptosis remain unclear.

Drawing upon the existing body of evidence, the present study aimed to characterize how varied aerobic-exercise intensities modulate renal ferroptosis in diabetic nephropathy. Accordingly, we established a type 2 diabetic nephropathy mouse model via a high-fat diet combined with streptozotocin (STZ) injection, and conducted 8-week interventions with different intensities of aerobic exercise. By examining the impacts of graded aerobic-exercise intensities on glucose metabolism, renal function and renal pathological damage in diabetic nephropathy mice, the present study sought to clarify the potential mechanism by which aerobic exercise alleviates diabetic nephropathy through regulating renal iron metabolism and ferroptosis. This study provides novel experimental evidence for the clinical application of aerobic exercise in the prevention and treatment of diabetic nephropathy.

2. Materials and Methods

2.1. Experimental Animals

Seventy-two specific pathogen-free (SPF) 8-week-old male C57BL/6J mice were purchased from SPF (Beijing) Biotechnology Co., Ltd (Beijing, China). All mice were housed in a standardized laboratory environment with constant temperature (25 ± 1 °C), constant humidity (55% ± 5%) and a 12 h light/dark cycle, with free access to food and drinking water. After one week of adaptive feeding, the mice were randomly divided into six groups ($n = 12$ per group): a control group (control), a diabetic nephropathy model group (model), a low-intensity aerobic-exercise group (LA), a moderate-intensity aerobic-exercise group (MA), a high-intensity aerobic-exercise group (HA), and a high-intensity interval training group (HIIT). The detailed workflow of the pilot experiment and formal animal studies is presented in Figures 1 and S1. All animal experiments were approved by the Animal Ethics Committee of Jianghan University and conducted in accordance with the ethical guidelines for laboratory animal care and use.

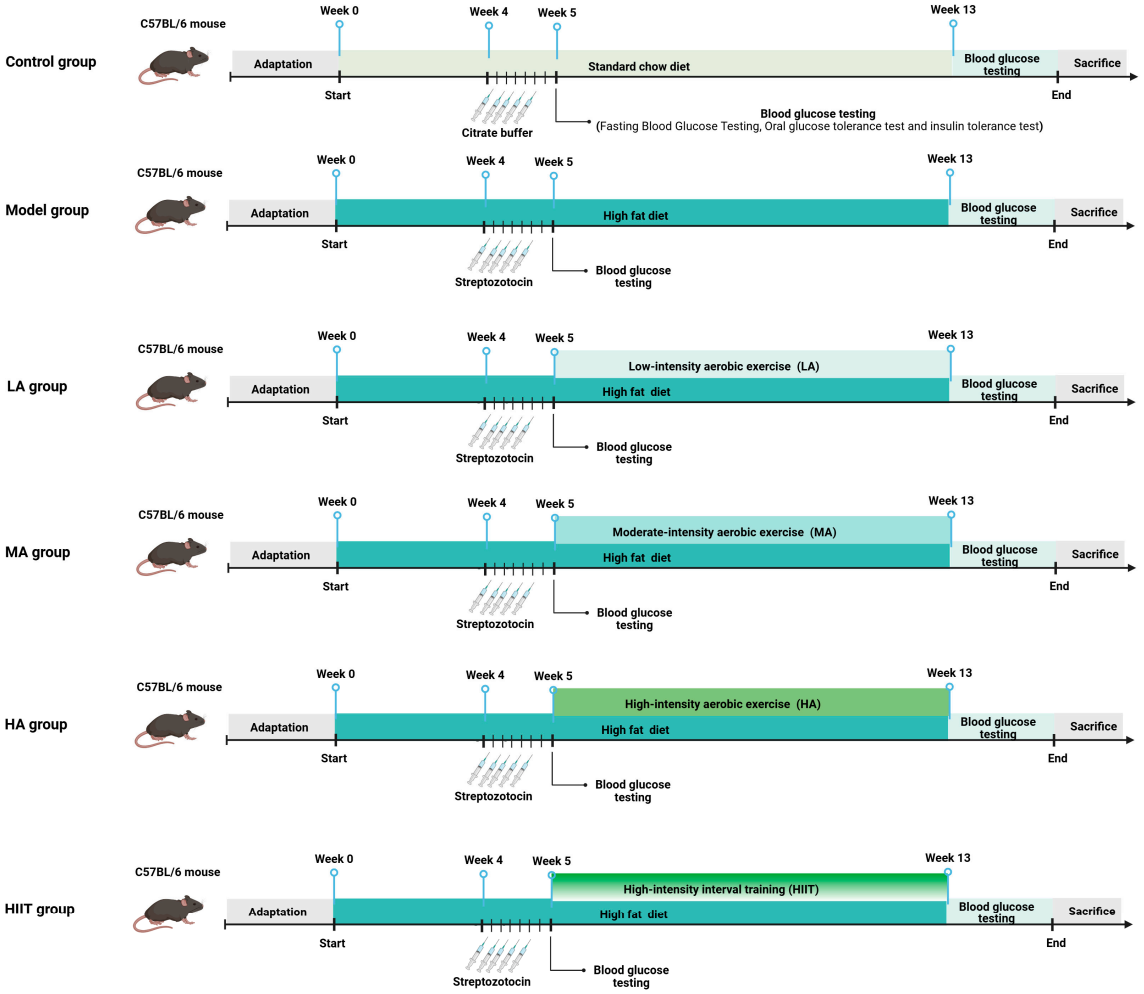


Figure 1. Schematic diagram of the animal experimental timeline.

2.2. Model Establishment

The animal model was established based on the pilot experiment (Figure S1) and the published literature [34]. Mice in the control group were fed with a standard chow diet, whereas the other five groups were fed with 60% high-fat diet (Jiangsu Xietong Pharmaceutical Bio-Engineering Co., Ltd., Nanjing, China). After 4 weeks of dietary feeding, mice in the model and all exercise groups received intraperitoneal injections of freshly prepared STZ (50 mg/kg) for 5 consecutive days, and mice in the control group were injected with an equal volume of citrate buffer (pH 4.5). To prevent STZ-induced hypoglycemia, glucose was supplemented in drinking water after injection. Fasting blood glucose (FBG) was detected on the 7th day after STZ injection. Mice with FBG $\geq$ 11.1 mmol/L, impaired glucose tolerance (evaluated by oral glucose tolerance test, OGTT), or insulin resistance (evaluated by insulin tolerance test, ITT), accompanied by typical symptoms such as polydipsia, polyphagia, polyuria and weight loss, were considered as successfully modeled, and maintained on the high-fat diet to sustain stable pathological conditions (Figure 1).

2.3. Exercise-Intervention Protocol

Before formal intervention, all exercise group mice received one week of adaptive treadmill training and underwent exhaustion tests to obtain individual maximal exhausted running speeds (Vmax). The reported maximal running speed of 16 m/min represents the group-averaged Vmax, and exercise speeds were calculated as a percentage of the group-averaged Vmax. The exercise intervention lasted for 8 weeks, 5 days a week, with

60 min each day, including 5 min warm-up + 50 min formal exercise + 5 min relaxation. The warm-up and relaxation speeds were 6 m/min. The exercise speeds of each group were set as percentages of Vmax (16 m/min): 6.4 m/min (40% Vmax) for the LA group, 9.6 m/min (60% Vmax) for the MA group, and 12.8 m/min (80% Vmax) for the HA group [35]. The HIIT group performed repeated cycles consisting of 60 s at 40% Vmax and 180 s at 80% Vmax. Mice in the control group and the model group did not receive any exercise intervention. The body weights of all mice were recorded weekly during the intervention period.

2.4. Sample Collection and Detection

2.4.1. Fasting Blood Glucose Testing

Before measurement, mice in each group were fasted for 12 h. The tail tips of the mice were cut off with sterilized surgical scissors, and blood was collected from the tail vein. The fasting blood glucose values of the mice were determined by Yuwell blood glucose meter. After the blood collection was completed, the tip of the mouse's tail was gently pressed with a sterile cotton swab for 30 to 60 s to stop the bleeding. Then, the mouse was put back into the cage and its diet resumed.

2.4.2. Glucose and Insulin Tolerance Test

Oral glucose tolerance test (OGTT) and insulin tolerance test (ITT) were conducted after model establishment and 8 weeks of intervention [36,37]. In OGTT, mice fasted for 12 h and received 20% glucose solution (2 g/kg body weight) by oral gavage. Blood glucose was measured at 0, 0.5, 1, 1.5 and 2 h after gavage, and the area under the blood glucose time curve (AUC) was calculated. In ITT, mice fasted for 12 h and were intraperitoneally injected with insulin (0.75 U/kg body weight). The blood glucose values at different time points were detected, and blood glucose at each time point was normalized to the 0 min baseline glucose and expressed as a percentage of the baseline value. The AUC was calculated based on these normalized values to assess insulin sensitivity, minimizing the confounding influence of variable individual baseline blood glucose levels.

2.4.3. Detection of Biochemical Indicators

After the intervention, mice were anesthetized and blood was collected. Serum was separated (4 °C, 3000 r/min, 10 min) and stored at −80 °C. The levels of serum glucose (GLU), glycated serum protein (GSP), insulin (INS), iron content, malondialdehyde (MDA), glutathione (GSH), blood urea nitrogen (BUN), uric acid (UA) and serum creatinine (Scr) were detected in accordance with the instructions of the kit (Nanjing Jiancheng Bioengineering Research Institute Co., Ltd., Nanjing, China). Renal tissue GSH and MDA were also quantified using commercial assay kits following the manufacturer's protocols. The homeostasis model assessment-insulin resistance (HOMA-IR) was calculated as GLU (mmol/L) × INS (mU/L)/22.5 [38]. Note: HOMA-IR was originally derived for human cohorts; in mouse models it serves only as a surrogate indicator and is not absolute gold-standard evidence for insulin resistance.

2.4.4. Renal Pathological Staining

The renal tissue was fixed with 4% paraformaldehyde, embedded in paraffin and then cut into 5 μm continuous sections. Hematoxylin–eosin (HE) staining was used to observe the general morphological changes in renal tissues, including the structure of glomeruli, the morphology of renal tubules and the infiltration of inflammatory cells. The degree of glomerular sclerosis and the degree of tubulointerstitial injury were evaluated by using periodic acid-Schiff (PAS) staining combined with a semi-quantitative scoring system [39]. For each sample, 20 glomeruli were randomly selected for glomerular sclerosis

scoring, and 10 fields of view were randomly observed at a magnification of 100× to assess tubulointerstitial injury. The average score of each sample was calculated. The specific scoring criteria are as follows: Glomerular sclerosis score: 0 points (normal glomerulus), 1 point (mesangial hyperplasia or sclerosis accounting for less than 25% of the glomerular area), 2 points (sclerosis affecting 25% to 50% of the glomerular area), and 3 points (sclerosis affecting 50% to 75% of the glomerular area). Renal tubulointerstitial injury score: 0 points (no obvious injury), 1 point (injury area < 25%), 2 points (injury area 25%~50%), and 3 points (injury area > 50%). Collagen fiber deposition in the renal interstitial was detected by Masson staining, and the volume fraction of collagen fibers was calculated to evaluate the degree of renal fibrosis [40].

2.4.5. Renal Iron Content Detection

Enhanced Prussian-blue staining was performed to observe and locate iron deposition in renal tissues. The total iron and ferrous ion contents in renal tissues were detected using commercial iron detection kits according to the manufacturer's protocols (Elabscience Biotechnology Co., Ltd., Wuhan, China). Renal tissues were homogenized on ice and centrifuged to obtain the supernatant, and the absorbance was measured at 593 nm to calculate total iron and ferrous ion levels.

2.4.6. Western Blot

Total protein was extracted from renal tissues using radio immunoprecipitation assay (RIPA) lysis buffer containing protease and phosphatase inhibitors (Servicebio Technology Co., Ltd., Wuhan, China). Protein concentration was determined by bicinchoninic acid (BCA) method (Servicebio Technology Co., Ltd., Wuhan, China), and protein denaturation was performed. After sodium dodecyl sulfate–polyacrylamide gel (SDS-PAGE) electrophoresis, membrane transfer and blocking, the membranes were incubated with primary antibodies against SLC39A14, GPX4, FTH, ACSL4, EPHX1, and β-actin (Boster Biological Technology Co., Ltd., Wuhan, China) overnight at 4 °C, followed by secondary antibody incubation for 1 h at room temperature. Finally, the protein bands were visualized by enhanced chemiluminescence (ECL) method (Servicebio Technology Co., Ltd., Wuhan, China), and the relative protein expression levels were analyzed by ImageJ software (version 1.53c; National Institutes of Health, Bethesda, MD, USA) with β-actin as the internal reference.

2.5. Bioinformatics Analysis of GEO Datasets

Three mouse diabetic nephropathy-related gene expression datasets, including GSE197699, GSE200322, and GSE280781, were downloaded from the Gene Expression Omnibus (GEO) database (https://www.ncbi.nlm.nih.gov/geo/, accessed on 7 April 2026). All datasets are mouse-origin datasets using renal whole-kidney tissue samples from control and diabetic nephropathy mice: GSE197699 (GPL24247, $n = 3$ per group); GSE200322 (GPL24247, $n = 6$ per group); and GSE280781 (GPL24247, $n = 5$ per group). Standardized bioinformatics analysis was performed using R software (version 4.2.1) and corresponding Bioconductor packages (GEOquery, limma, annotate, dplyr, VennDiagram) [41,42]. Specifically, the raw expression matrices of three GEO datasets were downloaded and probe IDs were converted to gene symbols. After normalization, differentially expressed genes (DEGs) between diabetic nephropathy and control groups were screened with the thresholds of $|\log2FC| > 1$ and adjusted p-value < 0.05 (Benjamini–Hochberg multiple-testing correction) [43]. Venn diagram analysis was subsequently conducted to intersect upregulated DEGs from the three independent datasets to identify consistently upregulated core genes in diabetic nephropathy. Shared upregulated DEGs were further intersected with FerrDb V3

database (access date: 10 March 2026), including four gene categories: Driver, Suppressor, Marker, and Unclassified. The full overlapping gene list is supplied in Supplementary Table S1. Among intersection candidates, EPHX1 was selected (annotated as Unclassified ferroptosis-related gene) and enriched in the arachidonic-acid metabolic pathway, with the published literature linking it to lipid peroxidation [24]. The key candidate gene epoxide hydrolase 1 (EPHX1) was finally determined.

2.6. Statistical Analysis

All experimental data were expressed as mean ± standard deviation (SD). SPSS 27.0 statistical software was used for data analysis. For longitudinal weekly body-weight data, mixed-effects models were applied, incorporating group, time, and group-by-time interaction terms. For OGTT and ITT, only AUC values were subjected to formal statistical comparisons; time-series line graphs are presented for descriptive visualization only and were not statistically analyzed. After testing the hypotheses of normality and homogeneity of variance, independent sample *t*-tests were conducted for the two groups of results, one-way analysis of variance was used for multiple groups of results, and then Tukey post hoc multiple comparisons were performed. Effect sizes were calculated to interpret the biological magnitude of observed differences. $p < 0.05$ was considered statistically significant. Complete statistical outputs for every measured endpoint are provided within the Supplementary Table S2.

3. Results

3.1. Effects of Different-Intensity Exercise on Body Weight, Hyperglycemia and Insulin Resistance in Type 2 Diabetic Nephropathy Mice

Prior to exercise intervention, body weight and glucose-metabolic phenotypes were assessed to validate successful establishment of the type 2 diabetic model. There was no significant difference in initial body weight among all groups before model establishment (Figure S2A). After high-fat-diet feeding combined with STZ injection, both the model and subsequent exercise groups exhibited significantly decreased body weight, elevated fasting blood glucose, aggravated glucose intolerance, and impaired insulin tolerance compared with the control group (Figure S2B–G). These data confirmed that diabetic phenotypes were stably induced.

To evaluate the renoprotective effects of different-intensity aerobic exercise against diabetic nephropathy, type 2 diabetic mice received an 8-week treadmill-based exercise intervention. Compared with the control group, the model group presented obvious hyperglycemia and insulin resistance, as evidenced by higher fasting blood glucose, deteriorated glucose and insulin tolerance, and an increased HOMA-IR index ($p < 0.01$). LA, MA, HA and HIIT ameliorated hyperglycemic phenotypes to varying degrees (Figure 2). Exercise interventions partially restored body weight and reduced fasting blood glucose, serum glucose, glycated serum protein and serum insulin levels. Consistently, improved glucose and insulin tolerance was reflected by decreased AUC values for OGTT and ITT, alongside a reduced HOMA-IR index ($p < 0.05$, Figures 2 and S3).

3.2. Effects of Different-Intensity Aerobic Exercise on Renal Function and Renal Pathological Injury in Type 2 Diabetic Nephropathy Mice

After 8-week treadmill exercise, renal index, serum renal-function biochemistry and renal histopathology were examined to clarify whether aerobic exercise mitigated renal damage in type 2 diabetic nephropathy mice. As illustrated in Figure 3A–D, the model group exhibited prominent renal dysfunction, with significantly higher renal index, serum urea nitrogen, serum uric acid and serum creatinine than the control group ($p < 0.01$).

Compared with the model group, LA, MA, HA and HIIT all reduced serum urea nitrogen, serum uric acid and serum creatinine to a statistically significant extent ($p < 0.01$).

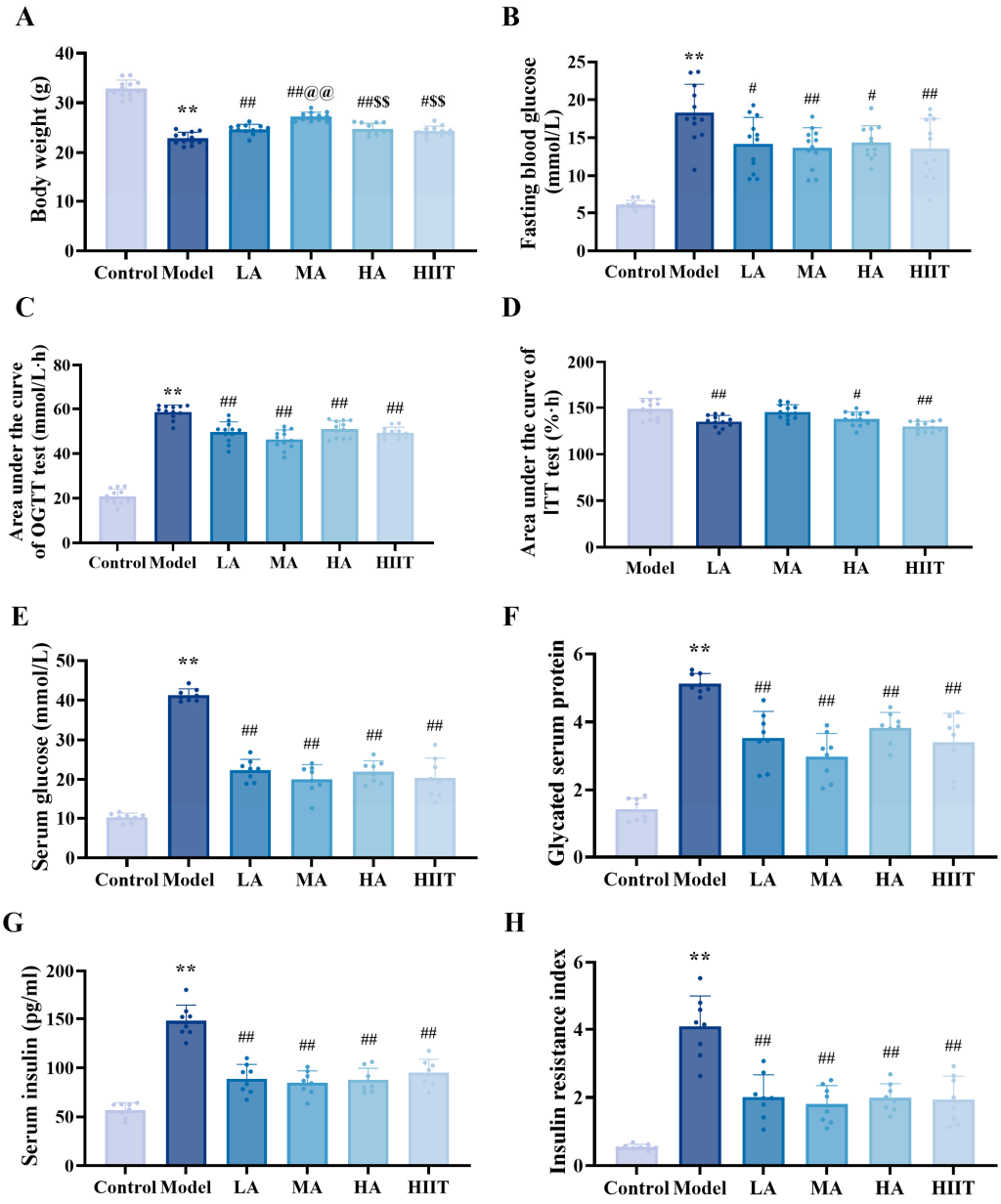


Figure 2. Different-intensity aerobic exercise ameliorates hyperglycemia and insulin resistance in type 2 diabetic nephropathy mice. (**A**) Body weight of mice in each group. (**B**) Fasting blood glucose (FBG) levels of mice in each group. (**C**) Area under the curve (AUC) values from oral glucose tolerance (OGTT) test. (**D**) AUC values from insulin tolerance (ITT) test. Data are presented as mean ± SD, $n = 12$ per group. (**E**) Fasting serum glucose levels in each group. (**F**) Glycated serum protein levels in each group. (**G**) Fasting insulin levels in each group. (**H**) Calculated HOMA-IR index reflecting insulin resistance status. Data are presented as mean ± SD, $n = 8$ per group. Compared with the control group, ** $p < 0.01$; compared with the model group, # $p < 0.05$, ## $p < 0.01$; compared with the LA group, @@ $p < 0.01$; compared with the MA group, $$ $p < 0.01$. Control, control group; Model, untreated diabetic model group; LA, low-intensity aerobic-exercise group; MA, moderate-intensity aerobic-exercise group; HA, high-intensity aerobic-exercise group; HIIT, high-intensity interval training group.

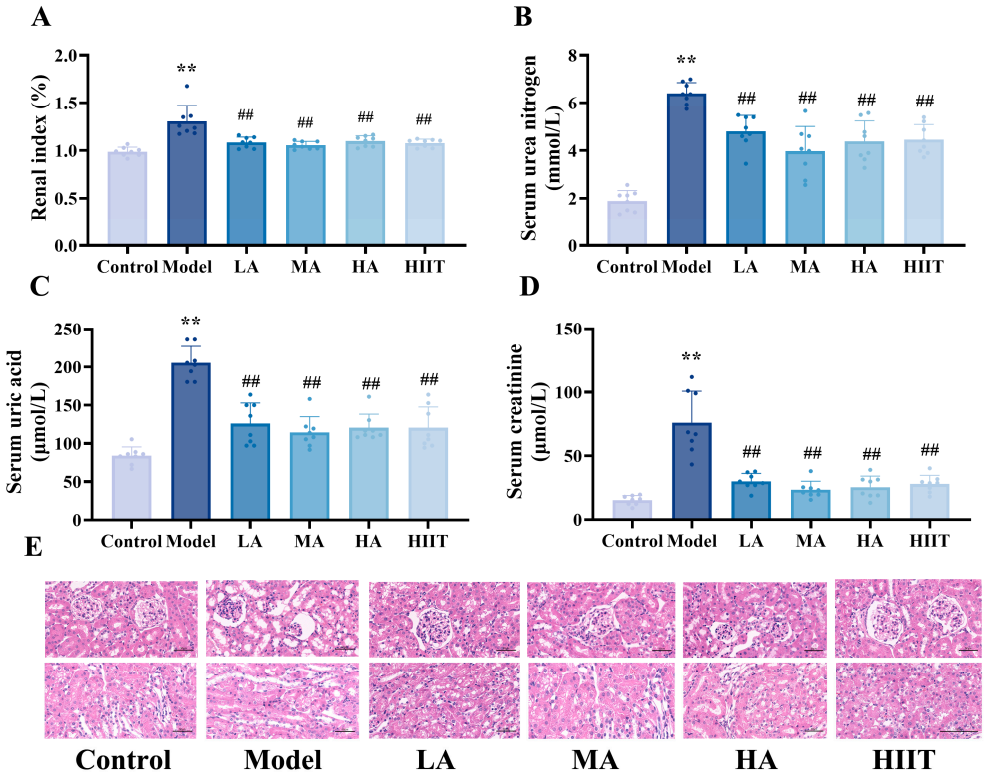


Figure 3. Effects of different-intensity aerobic exercise on renal function and renal histopathology in type 2 diabetic nephropathy mice. (**A**) Renal index. (**B**) Serum urea nitrogen. (**C**) Serum uric acid. (**D**) Serum creatinine. Data are presented as mean ± SD, $n = 8$ per group. (**E**) Representative HE-stained images of kidney tissues. Scale bar = 50 μm. Compared with the control group, ** $p < 0.01$; compared with the model group, ## $p < 0.01$.

HE staining was performed to evaluate renal morphological damage (Figure 3E). In the control group, glomerular and tubular structures remained intact, without basement-membrane hyperplasia, and glomerular capillary lumens were uniform. In contrast, the model group exhibited severe renal pathological alterations, such as enlarged Bowman's space, sparse and atrophic glomerular resident cells, compressed and irregular glomerular capillary loops, thickened glomerular-tubular basement membrane, loss of tubular brush border, dilated tubular lumen, vacuolar degeneration, atrophy and disorganized arrangement of tubular epithelial cells. Compared with the model group, all exercise-intervention groups displayed alleviated glomerular atrophy and mesangial proliferation. Collectively, these data demonstrated that different-intensity aerobic exercise could ameliorate renal dysfunction and mitigate renal structural damage in type 2 diabetic nephropathy mice.

3.3. Effects of Different-Intensity Aerobic Exercise on Glomerular and Tubular Injury and Renal Fibrosis in Type 2 Diabetic Nephropathy Mice

PAS staining was performed to evaluate glomerular and tubular structural damage (Figure 4A). The control group displayed a well-preserved glomerular architecture and basement membrane, uniform capillary lumens and orderly arranged renal tubules. In contrast, irregular dilation of Bowman's space, a thickened glomerular basement membrane, collapsed tubular lumens and a fractured tubular basement membrane were observed in the model group, indicating severe glomerular and tubular injury. Compared with the model group, all exercise-intervention groups showed markedly improved renal tissue architecture.

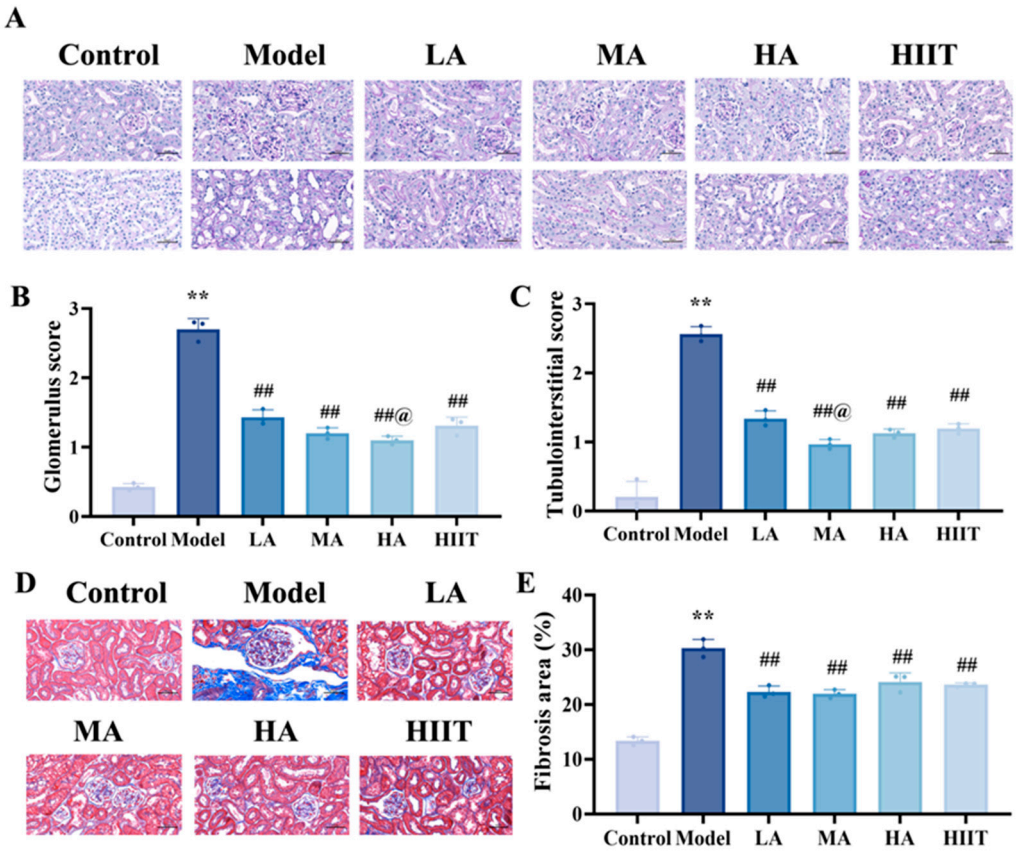


Figure 4. Effects of different-intensity aerobic exercise on renal histopathological injury and fibrosis in type 2 diabetic nephropathy mice. (**A**) Representative PAS-stained images of kidney tissues. (**B**) Glomerulosclerosis score. (**C**) Tubulointerstitial injury score. (**D**) Representative Masson trichrome-stained images of kidney tissues. (**E**) Quantitative analysis of renal fibrosis area (%). Scale bar = 50 μm. Data are expressed as mean ± SD, $n = 3$ per group. Compared with the control group, ** $p < 0.01$; compared with the model group, ## $p < 0.01$; compared with the LA group, @ $p < 0.05$.

Semi-quantitative scoring was further conducted to assess the severity of glomerulosclerosis and tubulointerstitial injury. As shown in Figure 4B, the glomerulosclerosis score was significantly elevated in the model group compared with the control group ($p < 0.01$). All exercise interventions significantly reduced the glomerulosclerosis score compared to the model group ($p < 0.01$), with the HA group exhibiting the most pronounced improvement. Similarly, the tubulointerstitial injury score was markedly increased in the model group ($p < 0.01$), and LA, MA, HA and HIIT all significantly lowered this score ($p < 0.01$, Figure 4C). These results indicated that different-intensity aerobic exercise could ameliorate both glomerulosclerosis and tubular injury in diabetic nephropathy mice.

Masson trichrome staining was used to detect collagen deposition and renal fibrosis (Figure 4D). The model group exhibited extensive diffuse collagen fiber deposition in the glomerular mesangial area, whereas collagen deposition was visibly reduced in all exercise-intervention groups. For quantitative analysis, the collagen fiber volume fraction was measured using ImageJ 1.53c software. As shown in Figure 4E, the collagen fiber volume fraction was significantly higher in the model group than in the control group ($p < 0.01$), indicating prominent renal fibrosis. Compared with the model group, LA, MA, HA and HIIT all significantly decreased the collagen fiber volume fraction ($p < 0.01$), demonstrating that different-intensity aerobic exercise could attenuate renal fibrosis in type 2 diabetic nephropathy mice.

3.4. Effects of Different-Intensity Aerobic Exercise on Renal Iron Deposition in Type 2 Diabetic Nephropathy Mice

Enhanced Prussian-blue staining was performed to evaluate iron deposition in renal tissues (Figure 5A). The renal tissues of the control group exhibited barely any brown-tan precipitates with low iron accumulation. By contrast, extensive brown-tan positive deposits were observed in the model group, indicating obvious renal iron overload in diabetic nephropathy mice. Compared with the model group, all exercise-intervention groups showed reduced brown-tan deposits, suggesting that aerobic exercise alleviated renal iron overload.

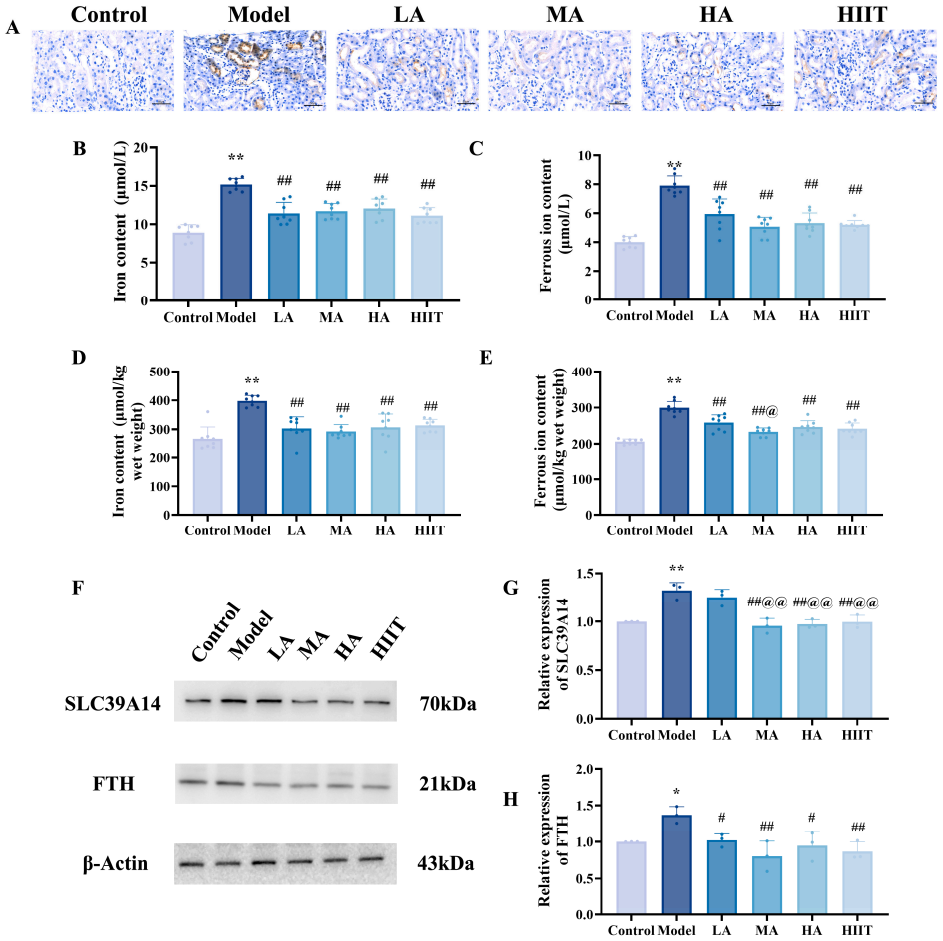


Figure 5. Effects of different-intensity aerobic exercise on renal iron deposition in diabetic nephropathy mice. (**A**) Representative enhanced Prussian-blue staining images of kidney sections. Scale bar = 50 μm. (**B**) Serum total iron content. (**C**) Serum ferrous ion content. (**D**) Renal total iron content. (**E**) Renal ferrous ion content. Data are presented as mean ± SD, $n = 8$ per group. (**F**–**H**) Western blot analysis and quantitative statistics of SLC39A14 and FTH protein expression. β-Actin served as the internal reference. Data are presented as mean ± SD, $n = 3$ per group. Compared with the control group, * $p < 0.05$, ** $p < 0.01$; compared with the model group, # $p < 0.05$, ## $p < 0.01$; compared with the LA group, @ $p < 0.05$, @@ $p < 0.01$.

Consistent with the histological staining results, renal total iron and ferrous ion levels were markedly elevated in the model group compared to the control group ($p < 0.01$). After exercise intervention, renal total iron content and ferrous ion content were significantly decreased in LA, MA, HA and HIIT groups compared with the model group ($p < 0.01$, Figure 5D,E). Similar changing trends were also observed for serum total iron and serum ferrous ion levels (Figure 5B,C).

To further explore the mechanism by which aerobic exercise regulates iron metabolism, Western blotting was used to detect the expression of iron metabolism-associated proteins SLC39A14 and FTH in kidney tissues (Figure 5F–H). Compared with the control group, SLC39A14 protein expression was significantly upregulated in the model group ($p < 0.01$). MA, HA and HIIT interventions markedly downregulated SLC39A14 protein expression compared to the model group ($p < 0.01$). Moreover, SLC39A14 levels in MA, HA and HIIT groups were significantly lower than those in the LA group ($p < 0.01$). For FTH protein expression, the model group exhibited a significant increase compared with the control group ($p < 0.05$). The LA, MA, HA and HIIT exercise groups all showed reduced FTH expression versus the model group. Specifically, FTH was significantly decreased in the LA and HA groups ($p < 0.05$), while MA and HIIT showed a more pronounced reduction ($p < 0.01$).

Taken together, these findings demonstrated disrupted iron homeostasis and prominent iron deposition in the kidneys of type 2 diabetic nephropathy mice. Different-intensity aerobic exercise could effectively restore abnormal iron metabolism and mitigate renal iron accumulation.

3.5. Effects of Different-Intensity Aerobic Exercise on Oxidative Stress in Type 2 Diabetic Nephropathy Mice

Serum GSH and MDA levels were determined using commercial kits to evaluate systemic antioxidant capacity and lipid peroxidation status. As shown in Figure 6A, serum GSH content was significantly decreased in the model group compared with the control group ($p < 0.01$). Compared to the model group, LA significantly elevated serum GSH levels ($p < 0.05$), while MA, HA and HIIT produced a significant increase ($p < 0.01$), indicating that aerobic exercise could effectively enhance the antioxidant capacity and ameliorate oxidative stress in diabetic nephropathy mice. As a marker of lipid peroxidation, serum MDA was significantly accumulated in the model group ($p < 0.01$). All four exercise interventions significantly reduced serum MDA content compared with the model group ($p < 0.01$, Figure 6B), suggesting that different-intensity aerobic exercise could effectively alleviate lipid peroxidation in diabetic nephropathy mice.

Renal GSH and MDA levels were detected to assess renal local antioxidant capacity and lipid peroxidation status. As shown in Figure 6C, renal GSH content was markedly reduced in the model group relative to the control group ($p < 0.01$). Compared with the model group, HA and HIIT induced a significant upregulation of renal GSH ($p < 0.05$), whereas no significant difference was observed in the LA and MA groups, demonstrating that aerobic exercise at higher intensities improved renal antioxidant capacity and mitigated renal oxidative stress in diabetic nephropathy mice. As a critical indicator of lipid peroxidation, renal MDA was significantly increased in the model group ($p < 0.01$). All four exercise interventions remarkably lowered renal MDA content when compared with the model group ($p < 0.01$, Figure 6D), indicating that aerobic exercise with different intensities could effectively relieve renal lipid peroxidation in diabetic nephropathy mice.

Western blotting was further performed to detect the expression of ferroptosis-associated proteins GPX4 and ACSL4 in renal tissues (Figure 6E–G). Compared with the control group, GPX4 protein expression was significantly downregulated in the model group ($p < 0.01$). After exercise intervention, MA and HA significantly upregulated GPX4 protein expression ($p < 0.05$), whereas HIIT exerted a significant restoring effect ($p < 0.01$, Figure 6F). In contrast, the protein level of ACSL4 was significantly increased in the model group ($p < 0.05$). MA, HA and HIIT groups showed a marked reduction in ACSL4 protein expression compared with the model group ($p < 0.01$, Figure 6G).

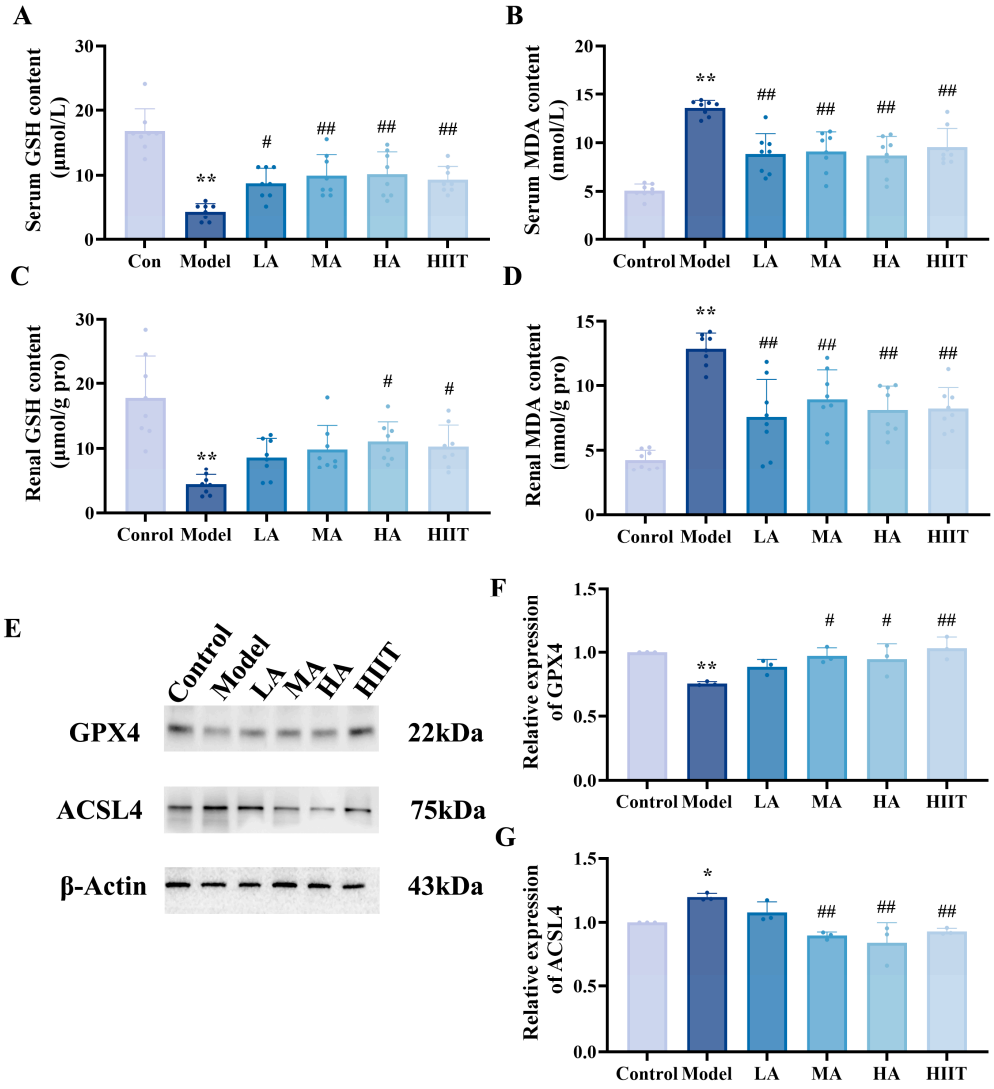


Figure 6. Effects of different-intensity aerobic exercise on oxidative stress and ferroptosis-related proteins in diabetic nephropathy mice. (**A**) Serum GSH content. (**B**) Serum MDA content. (**C**) Renal GSH content. (**D**) Renal MDA content. Data are presented as mean ± SD, $n = 8$ per group. (**E**) Representative Western blot bands of GPX4 and ACSL4. β-Actin served as the internal reference. (**F**) Quantitative analysis of relative GPX4 protein expression. (**G**) Quantitative analysis of relative ACSL4 protein expression. Data are presented as mean ± SD, $n = 3$ per group. Compared with the control group, * $p < 0.05$, ** $p < 0.01$; compared with the model group, # $p < 0.05$, ## $p < 0.01$.

Collectively, these results demonstrated that type 2 diabetic nephropathy mice suffered impaired antioxidant defense, enhanced lipid peroxidation, and dysregulated expression of ferroptosis-associated proteins. Different-intensity aerobic exercise could effectively ameliorate oxidative stress and renal pathological changes.

3.6. EPHX1-Arachidonic Acid Metabolism Pathway May Be Associated with Exercise-Alleviated Renal Ferroptosis in Type 2 Diabetic Nephropathy Mice

To identify candidate molecules mediating the protective effect of aerobic exercise against renal ferroptosis in type 2 diabetic nephropathy mice, three GEO datasets (GSE197699, GSE200322 and GSE280781) were analyzed to screen overlapping differentially expressed genes (Figure 7A,B). The shared upregulated genes were further intersected with the FerrDb V3 ferroptosis database (Figure 7C). Among the candidate

genes obtained from multiple intersection analyses, EPHX1 was selected for subsequent experimental verification.

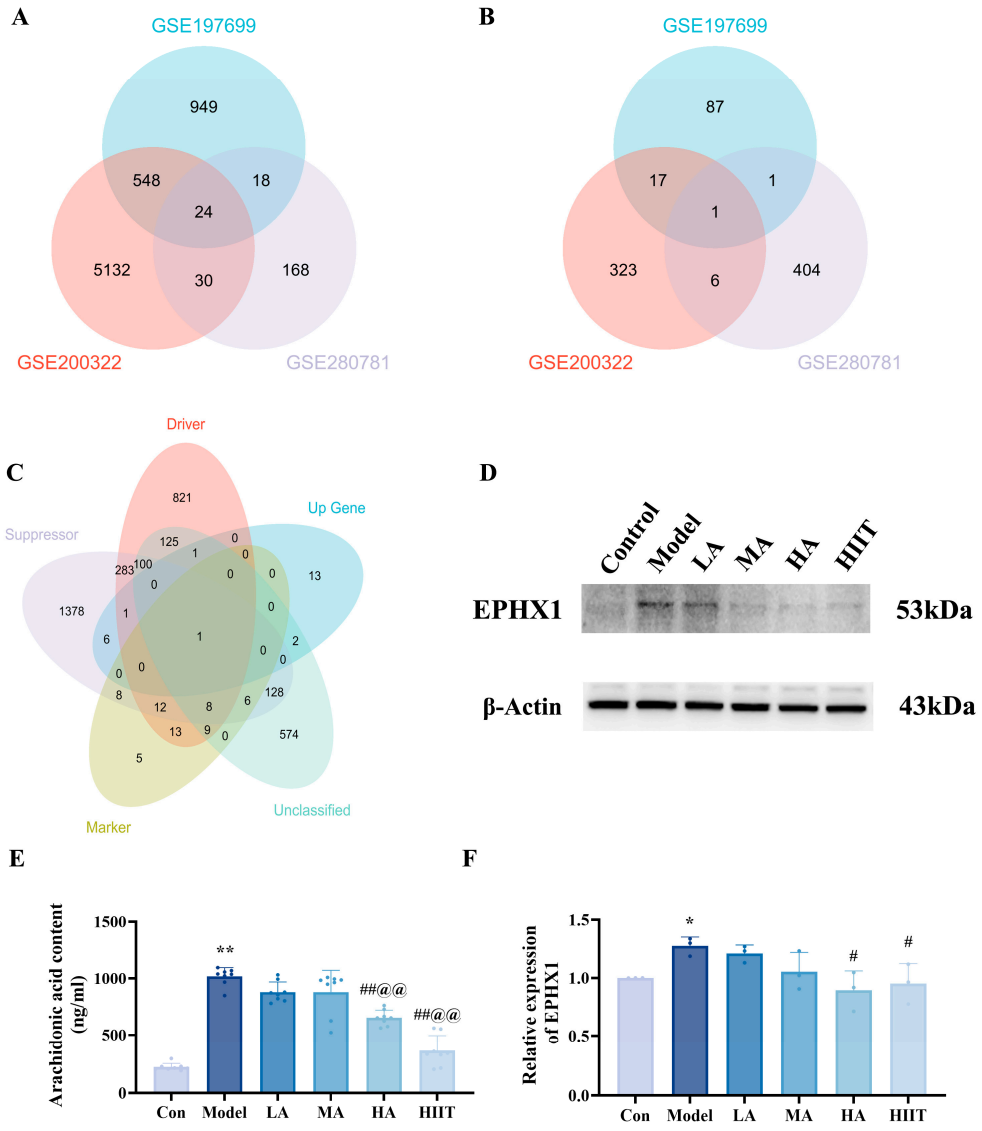


Figure 7. Bioinformatic screening and experimental validation of EPHX1 and arachidonic-acid metabolism. (**A**) Venn diagram illustrating the overlap of significantly upregulated differentially expressed genes (DEGs) derived from three mouse diabetic nephropathy GEO datasets (GSE197699, GSE200322, GSE280781). (**B**) Venn diagram showing the intersection of significantly downregulated DEGs across the three above-mentioned GEO datasets. (**C**) Venn diagram displaying the intersection of shared consistently upregulated DEGs (from panel A) against four functional gene categories (Driver, Suppressor, Marker, and Unclassified) obtained from the FerrDb V3 ferroptosis-related database. (**D**,**F**) Western blot detection and quantitative analysis of renal EPHX1 protein expression; β-Actin was used as internal reference. Data are presented as mean ± SD, $n = 3$ per group. (**E**) Renal arachidonic-acid content. Data are presented as mean ± SD, $n = 8$ per group. Compared with the control group, * $p < 0.05$, ** $p < 0.01$; compared with the model group, # $p < 0.05$, ## $p < 0.01$; compared with the LA group, @@ $p < 0.01$.

Compared with the control group, the EPHX1 protein level was significantly increased in the model group ($p < 0.05$, Figure 7D,F). Compared with the model group, EPHX1 expression was markedly downregulated in HA and HIIT exercise-intervention groups ($p < 0.05$). Arachidonic acid, the key substrate for lipid peroxidation during ferroptosis, was also detected. The model group exhibited sharply elevated renal arachidonic-acid

content ($p < 0.01$). Compared with the model group, arachidonic-acid levels were reduced in all exercise groups. LA and MA groups exhibited a decreasing trend without statistical significance, while HA and HIIT groups showed significant reductions ($p < 0.01$, Figure 7E).

These findings indicated that EPHX1 was upregulated in diabetic nephropathy kidneys, accompanied by the accumulation of arachidonic acid. Aerobic exercise downregulated EPHX1 expression and reduced arachidonic-acid abundance, which may represent one correlative mechanism whereby aerobic exercise suppresses molecular features associated with renal ferroptosis in type 2 diabetic nephropathy mice.

4. Discussion

Diabetic nephropathy is one of the most devastating microvascular complications of type 2 diabetes mellitus, which contributes to end-stage renal disease and imposes heavy clinical and socioeconomic burdens worldwide [44,45]. Hyperglycemia, insulin resistance, oxidative stress, abnormal iron metabolism and excessive lipid peroxidation jointly drive glomerulosclerosis, tubulointerstitial injury and renal fibrosis, ultimately leading to progressive renal-function decline [4,46–48]. Physical exercise has been recognized as a promising non-pharmacological intervention for diabetes and its complications [49,50]; nevertheless, the underlying molecular mechanisms by which different-intensity aerobic exercise alleviates diabetic nephropathy, especially its regulatory effects on renal ferroptosis, remain incompletely clarified. In the present study, we established a type 2 diabetic nephropathy mouse model via high-fat-diet feeding combined with STZ injection and systematically compared the renoprotective effects of 8-week low-intensity, moderate-intensity, and high-intensity aerobic treadmill exercise, as well as high-intensity interval training. Our results demonstrated that aerobic exercise ameliorated hyperglycemia and insulin resistance, improved renal function, and relieved glomerular-tubular pathological damage and renal fibrosis. Mechanistically, aerobic exercise restored renal iron homeostasis, mitigated oxidative stress and attenuated molecular features associated with renal ferroptosis. Further bioinformatic screening combined with in vivo validation identified that EPHX1-mediated arachidonic-acid metabolism may participate in exercise-triggered inhibition of renal ferroptosis-associated molecular alterations in diabetic nephropathy mice. Notably, HA and HIIT exhibited larger-magnitude phenotypic improvements relative to LA and MA, though pairwise statistical significance between exercise regimens was not achieved across all measured endpoints.

Consistent with previous reports, the type 2 diabetic nephropathy model mice exhibited typical diabetic manifestations, including body-weight loss, elevated fasting blood glucose, impaired glucose and insulin tolerance and increased HOMA-IR index [51,52]. Eight-week aerobic-exercise intervention partially restored metabolic disorders. All exercise regimens reduced fasting blood glucose, improved OGTT and ITT performance and decreased HOMA-IR index, confirming that aerobic exercise could alleviate systemic hyperglycemia and insulin resistance [53,54]. Hyperglycemia and insulin resistance are primary upstream drivers of renal injury in diabetic nephropathy [55,56]; the sustained high-glucose microenvironment induces glomerular hyperfiltration, basement-membrane thickening and tubular epithelial cell damage [57–59]. Therefore, the metabolic improvement induced by aerobic exercise provides a critical prerequisite for subsequent renal protection.

Renal-function indexes, including renal index, serum urea nitrogen, uric acid and creatinine, were significantly elevated in model mice, accompanied by typical histopathological changes such as glomerular capillary loop disorder and tubular epithelial vacuolar degeneration. Further PAS and Masson staining revealed prominent glomerulosclerosis, tubular injury and excessive collagen deposition, which recapitulate the core pathological features of clinical diabetic nephropathy [60]. Different-intensity aerobic exercise effectively

reversed renal dysfunction and alleviated glomerular-tubular injury as well as renal fibrosis. The existing literature has illustrated that exercise can suppress mesangial proliferation and extracellular-matrix accumulation in kidneys through inhibiting TGF-β-dependent fibrotic signaling pathways [61,62]. Our semi-quantitative scoring results showed that HA and HIIT achieved more obvious improvement in glomerulosclerosis, implying that appropriately increased exercise intensity may produce better renoprotection within a reasonable intensity window.

Ferroptosis is increasingly considered a vital pathogenic factor of various diseases [11,63]. Excessive iron deposition catalyzes reactive oxygen species production via Fenton reaction, amplifies oxidative damage and triggers cell-death signaling, thereby aggravating renal injury [64–66]. In our study, enhanced Prussian-blue staining demonstrated massive iron accumulation in the kidneys of diabetic nephropathy mice, accompanied by significant increases in total iron and ferrous ion in both serum and renal tissues. The iron-transport-related protein SLC39A14 and iron-storage protein FTH were also significantly upregulated, indicating disrupted renal iron homeostasis. SLC39A14 is responsible for cellular ferrous ion uptake, and its overexpression promotes intracellular iron influx and iron overload [67,68]. FTH represents the ferritin heavy-chain protein; altered FTH expression reflects changes in iron-storage status, and elevated FTH reflects compensatory iron storage under iron-overload conditions [69,70]. After aerobic-exercise intervention, iron deposition was markedly attenuated, serum and renal iron levels declined, and SLC39A14 and FTH expression were downregulated. These observations suggested that aerobic exercise could relieve renal iron overload by modulating iron-uptake and iron-storage proteins, which is consistent with earlier studies reporting that exercise remodels systemic iron metabolism in diabetic conditions [33,71].

Ferroptosis is characterized by GSH depletion, GPX4 inactivation and ACSL4-driven lipid peroxidation, and accumulating evidence highlights the pivotal role of ferroptosis in the progression of diabetic nephropathy [72–74]. In our experiment, diabetic nephropathy mice displayed obvious oxidative-stress imbalance, including decreased serum GSH, increased MDA, downregulated GPX4 and upregulated ACSL4 in renal tissues. GPX4 is the core anti-ferroptosis enzyme that relies on GSH to detoxify lipid peroxides, while ACSL4 catalyzes the synthesis of polyunsaturated-fatty-acid-containing phospholipids, which are essential substrates for lipid peroxidation and ferroptosis execution [75,76]. Aerobic exercise elevated serum GSH, reduced MDA content, restored GPX4 expression and suppressed ACSL4 abundance, indicating that aerobic exercise attenuates molecular features associated with renal ferroptosis by enhancing antioxidant capacity and restraining lipid peroxidation. Among the four exercise modes, HA and HIIT exerted more prominent effects on GPX4 recovery, further explaining their superior protective effects against renal pathological damage.

To further explore potential regulatory molecules linking aerobic exercise and ferroptosis inhibition, we performed an intersection analysis of three GEO diabetic nephropathy datasets combined with the FerrDb V3 ferroptosis database and screened out candidate molecule EPHX1 [23]. In our diabetic nephropathy renal model, we observed parallel increases in renal EPHX1 protein and arachidonic-acid levels. We hypothesized that the upregulation of EPHX1 would alter the lipid balance of arachidonic acid, EETs, DHET, and the membrane-esterified polyunsaturated fatty acid-phospholipid pools in renal tissue, thereby affecting the storage pool of lipid peroxides and increasing the sensitivity of renal cells to ferroptosis. Aerobic exercise, especially HA and HIIT, downregulated EPHX1 and reduced arachidonic-acid accumulation. Previous studies have reported that EPHX1 dysregulation disturbs arachidonic-acid-derived lipid mediator homeostasis and exacerbates oxidative tissue injury [24]. Accordingly, we reasonably speculate that aerobic exercise may re-

verse ferroptosis-associated molecular alterations partially via inhibiting EPHX1-dependent arachidonic-acid accumulation, so as to mitigate renal damage in diabetic nephropathy.

Nevertheless, the present study still has several important limitations that should be acknowledged when interpreting our findings. First, all experiments were performed using animal models only. Direct gene-modulation approaches, such as gene knockout or overexpression assays, are still required to definitively verify the causal relationship between EPHX1 and exercise-mediated anti-ferroptosis effects in the kidney, rather than merely establishing correlative associations. Furthermore, the homeostasis of peroxides in the kidneys is regulated by multiple metabolic pathways. The current research results only support one correlation hypothesis, that is, that EPHX1 is associated with renal lipid remodeling and ferroptosis. Therefore, it is necessary to conduct further research by integrating lipidomics targeting the kidneys with experiments on the gain or loss of EPHX1 function, in order to verify the role of this signaling pathway in diabetic nephropathy. Second, it is noteworthy that all exercise regimens applied in this study induced measurable improvements in systemic glucose and insulin responses. As such, we cannot fully disentangle whether exercise inhibits renal ferroptosis-associated molecular features through direct modulation of intrarenal signaling pathways, or whether the observed renal protective phenotypes arise secondarily from the amelioration of whole-body glucose homeostasis. Future studies employing kidney-specific genetic manipulation may help dissociate the direct renal actions of exercise from systemic metabolism-mediated secondary effects. Third, only male C57BL/6J mice were used in the present study. Given known sex-divergent susceptibility to renal injury and ferroptosis, our results cannot be extrapolated to female animals. In addition, the translational potential of our findings remains to be validated. Further clinical investigations are needed to examine whether exercise can regulate EPHX1 expression and arachidonic-acid metabolism in patients with diabetic nephropathy, and to determine whether similar anti-ferroptosis mechanisms are operative in diabetic nephropathy patients.

5. Conclusions

Although accumulating evidence has confirmed the critical pathogenic role of ferroptosis in the progression of diabetic nephropathy, most existing studies focus on pharmacological interventions targeting ferroptosis [77–79], whereas direct in vivo experimental evidence linking exercise-mediated renal protection to ferroptosis suppression remains relatively limited, especially regarding comparisons among different aerobic-exercise intensities. In this context, our present study systematically compared the renoprotective effects of LA, MA and HA, as well as HIIT in type 2 diabetic nephropathy mice. We demonstrated that different-intensity aerobic exercise, particularly HA and HIIT, improved hyperglycemia and insulin resistance, rescued renal function, and alleviated glomerular-tubular injury and renal fibrosis. Mechanistically, these protective effects were closely associated with restoring iron homeostasis, improving antioxidant capacity, inhibiting lipid peroxidation and attenuating molecular features associated with renal ferroptosis. EPHX1-dependent arachidonic-acid metabolism acts as a potential downstream regulatory axis underlying exercise-mediated renoprotection. Collectively, our findings provide novel experimental supplements for understanding the protective mechanism of exercise and offer an experimental basis and mechanistic reference for applying aerobic exercise as a non-invasive therapeutic strategy for diabetic nephropathy.

Supplementary Materials: The following supporting information can be downloaded at https://www.mdpi.com/article/10.3390/biology15222118/s1, Figure S1: Establishment of type 2 diabetic nephropathy mouse model. (A) Schematic diagram of the pilot experimental timeline. (B) Body weight of mice at week 1 and week 12. (C) Fasting blood glucose levels at week 1 and week 12. (D) Blood glucose curve of oral glucose tolerance (OGTT) test. (E) Area under the curve (AUC) of OGTT.

Data are presented as mean ± SD, $n = 10$ per group. (F–G) Representative Hematoxylin-eosin (HE) staining images of kidney tissues from control group (F) and model group (G). Scale bar = 20 μm; Data are presented as mean ± SD. Compared with the control group, ** $p < 0.01$; Figure S2: Verification of type 2 diabetic model establishment prior to exercise intervention. (A) Baseline body weight of mice before model establishment. (B–G) Physiological indexes detected after high-fat diet and STZ injection. (B) Body weight; (C) Fasting blood glucose; (D,E) Blood-glucose curves and AUC values of the OGTT test; (F,G) Blood-glucose curves and AUC values of the ITT test. Data are presented as mean ± SD, $n = 12$ per group. Compared with the control group, ** $p < 0.01$. Control, control group; Model, untreated diabetic model group; LA, low-intensity aerobic exercise group; MA, moderate-intensity aerobic exercise group; HA, high-intensity aerobic exercise group; HIIT, high-intensity interval training group; Figure S3: Different-intensity aerobic exercise ameliorates hyperglycemia in type 2 diabetic nephropathy mice. (A) Dynamic blood glucose curve from oral glucose tolerance (OGTT) test. (B) Dynamic blood glucose curves from insulin tolerance (ITT) test. Data are presented as mean ± SD, $n = 12$ per group. Table S1: Bioinformatics analysis. Table S2: Statistical analysis results.

Author Contributions: All authors contributed to the study conception and design. Q.R. and X.X. designed the study. X.X. and B.C. developed the methodology. C.X. performed formal data analysis. Q.R. and X.X. curated and validated the raw data. Q.R. wrote the original draft of the manuscript. L.C. and Y.W. revised and edited the manuscript. All authors have read and agreed to the published version of the manuscript.

Funding: This work was supported by grants from the National Natural Science Foundation of China (No. 82672053) and Basic Research Project of Jianghan University (No. 2025JCYJ07).

Institutional Review Board Statement: All animal experiments were conducted in strict accordance with the National Institutes of Health Guide for the Care and Use of Laboratory Animals and were approved by the Animal Care and Use Committee of Jianghan University (Approval ID: JHDXLL2024-052, Approval date: 10 March 2024). All procedures involving animals were performed under full compliance with institutional ethical guidelines and were regularly monitored to ensure animal welfare.

Data Availability Statement: The dataset supporting the conclusions of this article is included within the article. Statistical analysis results and bioinformatics analysis results are provided in the Supplementary Materials. Supplementary Figures S1–S3 together with complete formal legends are included in the Supplementary Materials.

Conflicts of Interest: The authors declare no conflicts of interest.

References

1. Niu, F.; Liu, W.; Ren, Y.; Tian, Y.; Shi, W.; Li, M.; Li, Y.; Xiong, Y.; Qian, L. beta-cell neogenesis: A rising star to rescue diabetes mellitus. *J. Adv. Res.* **2024**, *62*, 71–89. [CrossRef] [PubMed]
2. Tomic, D.; Shaw, J.E.; Magliano, D.J. The burden and risks of emerging complications of diabetes mellitus. *Nat. Rev. Endocrinol.* **2022**, *18*, 525–539. [CrossRef] [PubMed]
3. Martinez Leon, V.; Hilburg, R.; Susztak, K. Mechanisms of diabetic kidney disease and established and emerging treatments. *Nat. Rev. Endocrinol.* **2026**, *22*, 21–35. [CrossRef] [PubMed]
4. Tuttle, K.R.; Agarwal, R.; Alpers, C.E.; Bakris, G.L.; Brosius, F.C.; Kolkhof, P.; Uribarri, J. Molecular mechanisms and therapeutic targets for diabetic kidney disease. *Kidney Int.* **2022**, *102*, 248–260. [CrossRef] [PubMed]
5. Cleveland, K.H.; Schnellmann, R.G. Pharmacological Targeting of Mitochondria in Diabetic Kidney Disease. *Pharmacol. Rev.* **2023**, *75*, 250–262. [CrossRef] [PubMed]
6. Rayego-Mateos, S.; Rodrigues-Diez, R.R.; Fernandez-Fernandez, B.; Mora-Fernandez, C.; Marchant, V.; Donate-Correa, J.; Navarro-Gonzalez, J.F.; Ortiz, A.; Ruiz-Ortega, M. Targeting inflammation to treat diabetic kidney disease: The road to 2030. *Kidney Int.* **2023**, *103*, 282–296. [CrossRef] [PubMed]
7. Bavanandan, S.; Noronha, I.L.; Tchokhonelidze, I.; Liew, A. Metabolic disorder-associated kidney disease and diabetic kidney disease in developing countries. *Kidney Int.* **2025**, *108*, 380–387. [CrossRef] [PubMed]
8. Sun, X.; Jiang, Y.; Wang, H.; Wang, Z.; Sun, W.; Liu, Y. A bibliometric analysis of trace elements and diabetic kidney disease: Scientific hotspots and research evolution. *Ren. Fail.* **2026**, *48*, 2736897. [CrossRef] [PubMed]

9. Zang, H.; Zang, F.; Zhang, H.; Lei, Y.; Jiang, Y.; Li, Y.; Tang, D.; Wang, D.; Xiao, F. BRD2-Mediated TGR5 destabilization impairs fatty acid oxidation and drives tubular ferroptosis in diabetic kidney injury. *Free Radic. Biol. Med.* **2026**, *256*, 357–374. [CrossRef] [PubMed]
10. Sanz, A.B.; Sanchez-Nino, M.D.; Ramos, A.M.; Ortiz, A. Regulated cell death pathways in kidney disease. *Nat. Rev. Nephrol.* **2023**, *19*, 281–299. [CrossRef] [PubMed]
11. Ru, Q.; Li, Y.; Chen, L.; Wu, Y.; Min, J.; Wang, F. Iron homeostasis and ferroptosis in human diseases: Mechanisms and therapeutic prospects. *Signal Transduct. Target. Ther.* **2024**, *9*, 271. [CrossRef] [PubMed]
12. Dixon, S.J.; Olzmann, J.A. The cell biology of ferroptosis. *Nat. Rev. Mol. Cell Biol.* **2024**, *25*, 424–442. [CrossRef] [PubMed]
13. Sun, S.; Shen, J.; Jiang, J.; Wang, F.; Min, J. Targeting ferroptosis opens new avenues for the development of novel therapeutics. *Signal Transduct. Target. Ther.* **2023**, *8*, 372. [CrossRef] [PubMed]
14. Xu, F.; Jiang, H.; Li, X.; Pan, J.; Li, H.; Wang, L.; Zhang, P.; Chen, J.; Qiu, S.; Xie, Y.; et al. Discovery of PRDM16-Mediated TRPA1 Induction as the Mechanism for Low Tubulo-Interstitial Fibrosis in Diabetic Kidney Disease. *Adv. Sci.* **2024**, *11*, e2306704. [CrossRef] [PubMed]
15. Hong, J.; Xu, H.; Yu, L.; Yu, Z.; Chen, X.; Meng, Z.; Zhu, J.; Li, J.; Zhu, M. AARS1-mediated lactylation of H3K18 and STAT1 promotes ferroptosis in diabetic nephropathy. *Cell Death Differ.* **2026**, *33*, 589–604. [CrossRef] [PubMed]
16. Tian, S.; Zhou, S.; Wu, W.; Lin, Y.; Wang, T.; Sun, H.; A-Ni-Wan, A.-S.-J.; Li, Y.; Wang, C.; Li, X.; et al. GLP-1 Receptor Agonists Alleviate Diabetic Kidney Injury via beta-Klotho-Mediated Ferroptosis Inhibition. *Adv. Sci.* **2025**, *12*, e2409781. [CrossRef] [PubMed]
17. Liao, P.; Wang, W.; Wang, W.; Kryczek, I.; Li, X.; Bian, Y.; Sell, A.; Wei, S.; Grove, S.; Johnson, J.K.; et al. CD8(+) T cells and fatty acids orchestrate tumor ferroptosis and immunity via ACSL4. *Cancer Cell* **2022**, *40*, 365–378.e366. [CrossRef] [PubMed]
18. Zhang, X.; Xu, Y.; Ma, L.; Yu, K.; Niu, Y.; Xu, X.; Shi, Y.; Guo, S.; Xue, X.; Wang, Y.; et al. Essential roles of exosome and circRNA_101093 on ferroptosis desensitization in lung adenocarcinoma. *Cancer Commun.* **2022**, *42*, 287–313. [CrossRef] [PubMed]
19. Shi, Z.; He, Z.; Wang, D.W. CYP450 Epoxygenase Metabolites, Epoxyeicosatrienoic Acids, as Novel Anti-Inflammatory Mediators. *Molecules* **2022**, *27*, 3873. [CrossRef] [PubMed]
20. Spector, A.A. Arachidonic acid cytochrome P450 epoxygenase pathway. *J. Lipid Res.* **2009**, *50*, S52–S56. [CrossRef] [PubMed]
21. Newman, J.W.; Morisseau, C.; Hammock, B.D. Epoxide hydrolases: Their roles and interactions with lipid metabolism. *Prog. Lipid Res.* **2005**, *44*, 1–51. [CrossRef] [PubMed]
22. Liu, Y.; Lu, M.; Du, Y.; Xu, J.; Fan, M.; Xue, C.; Liu, Y. Time-of-Day Defines the Risk of Thermally Abused Frying Oil to Renal Injury by Modulating the Diurnal Dynamics of Oxylipins. *Exploration* **2026**, *6*, 20240073. [CrossRef] [PubMed]
23. Zhu, H.; Zikela, L.; Wang, D.; Yu, Z.; Zhu, Y.; Zhou, H.; Li, X.; Wu, Y.; Han, Q. Nobiletin alleviates alcoholic fatty liver disease by regulating lipid metabolism and oxidative stress via Ephx1 and Sult1a1. *Phytomedicine* **2026**, *153*, 157977. [CrossRef] [PubMed]
24. Fan, X.; Dai, Y.; Mo, C.; Li, H.; Luan, X.; Wang, B.; Yang, J.; Jiao, G.; Lu, X.; Chen, Z.; et al. TRIM21 Promotes Tumor Growth and Gemcitabine Resistance in Pancreatic Cancer by Inhibiting EPHX1-Mediated Arachidonic Acid Metabolism. *Adv. Sci.* **2025**, *12*, e2413674. [CrossRef] [PubMed]
25. Ma, X.H.; Liu, J.H.; Liu, C.Y.; Sun, W.Y.; Duan, W.J.; Wang, G.; Kurihara, H.; He, R.R.; Li, Y.F.; Chen, Y.; et al. ALOX15-launched PUFA-phospholipids peroxidation increases the susceptibility of ferroptosis in ischemia-induced myocardial damage. *Signal Transduct. Target. Ther.* **2022**, *7*, 288. [CrossRef] [PubMed]
26. Martin-Saiz, L.; Guerrero-Mauvecin, J.; Martin-Sanchez, D.; Fresnedo, O.; Gomez, M.J.; Carrasco, S.; Cannata-Ortiz, P.; Ortiz, A.; Fernandez, J.A.; Sanz, A.B. Ferrostatin-1 modulates dysregulated kidney lipids in acute kidney injury. *J. Pathol.* **2022**, *257*, 285–299. [CrossRef] [PubMed]
27. Chen, Y.; Chen, Z.; Pan, L.; Ma, Z.M.; Zhang, H.; Li, X.J.; Li, X. Effect of Moderate and Vigorous Aerobic Exercise on Incident Diabetes in Adults With Obesity: A 10-Year Follow-up of a Randomized Clinical Trial. *JAMA Intern. Med.* **2023**, *183*, 272–275. [CrossRef] [PubMed]
28. Mucinski, J.M.; Salvador, A.F.; Moore, M.P.; Fordham, T.M.; Anderson, J.M.; Shryack, G.; Cunningham, R.P.; Lastra, G.; Gaballah, A.H.; Diaz-Arias, A.; et al. Histological improvements following energy restriction and exercise: The role of insulin resistance in resolution of MASH. *J. Hepatol.* **2024**, *81*, 781–793. [CrossRef] [PubMed]
29. Garcia-Hermoso, A.; Lopez-Gil, J.F.; Izquierdo, M.; Ramirez-Velez, R.; Ezzatvar, Y. Exercise and Insulin Resistance Markers in Children and Adolescents With Excess Weight: A Systematic Review and Network Meta-Analysis. *JAMA Pediatr.* **2023**, *177*, 1276–1284. [CrossRef] [PubMed]
30. Michou, V.; Tsamos, G.; Vasdeki, D.; Kouidi, E.; Deligiannis, A. Diabetic kidney disease and cardiac autonomic neuropathy: Insights on exercise rehabilitation. *J. Nephrol.* **2025**, *38*, 457–471. [CrossRef] [PubMed]
31. Monno, I.; Ogura, Y.; Xu, J.; Koya, D.; Kitada, M. Exercise Ameliorates Diabetic Kidney Disease in Type 2 Diabetic Fatty Rats. *Antioxidants* **2021**, *10*, 1754. [CrossRef] [PubMed]
32. Felix-Soriano, E.; Stanford, K.I. Exerkines and redox homeostasis. *Redox Biol.* **2023**, *63*, 102748. [CrossRef] [PubMed]

33. Plaza-Florido, A.; Lucia, A.; Fiuza-Luces, C. Exercise is also medicine for iron homeostasis. *Trends Endocrinol. Metab.* **2024**, *35*, 180–182. [CrossRef] [PubMed]
34. Han, Y.C.; Tang, S.Q.; Liu, Y.T.; Li, A.M.; Zhan, M.; Yang, M.; Song, N.; Zhang, W.; Wu, X.Q.; Peng, C.H.; et al. AMPK agonist alleviate renal tubulointerstitial fibrosis via activating mitophagy in high fat and streptozotocin induced diabetic mice. *Cell Death Dis.* **2021**, *12*, 925. [CrossRef] [PubMed]
35. Zhou, X.; Wang, D.; Deng, H.; Guo, J.; Chen, X.; Lin, Z.; Liu, B.; Zhao, R.; Gao, L.; Yin, X.; et al. Myokine Cathepsin B as a Key Muscle-Brain Axis Regulator Mediates Treadmill-Running-Induced Hippocampal Neurogenesis and Cognitive Improvement in Mice. *Research* **2026**, *9*, 1233. [CrossRef] [PubMed]
36. Liu, R.; She, J.; Li, X.; Yan, Y.; Mo, J.; Sheng, J.; Yang, H.; Huang, H. Multi-Omics Revealed the Effects of Intrauterine Hyperglycemia Exposure on the Development of Skeletal Muscle in Offspring. *J. Cachexia Sarcopenia Muscle* **2026**, *17*, e70177. [CrossRef] [PubMed]
37. Kim, J.W.; Lee, J.; You, Y.H.; Oh, C.H.; Park, H.S.; Lee, E.Y.; Lee, S.H.; Ko, S.H.; Park, J.H.; Yoon, K.H. Targeting PGC-1alpha by miRNA-374 Simultaneously Improve beta-Cell Dysfunction and Suppress Hepatic Glucose Overproduction. *Diabetes Metab. J.* **2026**, *50*, 535–551. [CrossRef] [PubMed]
38. Wang, S.; Shi, J.; Peng, Y.; Fang, Q.; Mu, Q.; Gu, W.; Hong, J.; Zhang, Y.; Wang, W. Stronger association of triglyceride glucose index than the HOMA-IR with arterial stiffness in patients with type 2 diabetes: A real-world single-centre study. *Cardiovasc. Diabetol.* **2021**, *20*, 82. [CrossRef] [PubMed]
39. Hu, J.; Pang, X.; Liang, X.; Shao, X.; Xia, Q.; Sun, J.; Wang, Y.; Wang, G.; Li, S.; Zha, L.; et al. Raspberry ameliorates renal fibrosis in rats with chronic kidney disease via the PI3K/Akt pathway. *Phytomedicine* **2025**, *140*, 156589. [CrossRef] [PubMed]
40. Zhang, S.; Wen, Z.; Chen, Y.; Yang, Y.; Song, C.; Wang, J.; Zhou, Y.; Ni, Q. Keluoxin reduces renal lipid deposition in diabetic nephropathy via AMPK/NF-kappaB-mediated metabolic regulation. *Phytomedicine* **2025**, *145*, 156776. [CrossRef] [PubMed]
41. Luo, Y.; Song, Y.; Zeng, M.; Li, B.; Li, Y.; Dong, Z. The past, present, and future of adipose tissue browning and aging: A review combined with bibliometrics and bioinformatics of 2527 documents published over the past four decades. *Ageing Res. Rev.* **2026**, *114*, 102959. [CrossRef] [PubMed]
42. Ye, S.; Zhang, M.; Zheng, X.; Li, S.; Fan, Y.; Wang, Y.; Peng, H.; Chen, S.; Yang, J.; Tan, L.; et al. YAP1 preserves tubular mitochondrial quality control to mitigate diabetic kidney disease. *Redox Biol.* **2024**, *78*, 103435. [CrossRef] [PubMed]
43. Guadalupe-Grau, A.; Gudra, D.; Lismane, D.; Raudeniece, J.; Akuratere, G.; Viksne, K.; Gailite, L.; Vilne, B.; Pivovarova-Ramich, O.; Flensted-Jensen, M.; et al. Skeletal Muscle Transcriptomic Responses to Concurrent Training With Polyphenols in Ageing Adults: A Randomized Trial. *J. Cachexia Sarcopenia Muscle* **2026**, *17*, e70391. [CrossRef] [PubMed]
44. Liu, J.; Tan, X.; Fang, X.; Ge, X.; Xu, L.; Long, Y.; Mao, X.; Xu, Y. Deubiquitinating enzymes as therapeutic targets in diabetic nephropathy. *Trends Pharmacol. Sci.* **2026**, *47*, 198–215. [CrossRef] [PubMed]
45. Pruijm, M.; Belmar, N.; Bjornstad, P.; Cherney, D.Z.I.; Das, V.; Gunnarsson, T.; Hodgin, J.B.; Schytz, P.A.; Tuttle, K.R.; Kretzler, M. REMODELing mechanistic trials for kidney disease: A multimodal, tissue-centered approach to understand the renal mechanism of action of semaglutide. *Kidney Int.* **2026**, *109*, 6–16. [CrossRef] [PubMed]
46. Xuan, C.; Chen, D.; Zhang, S.; Li, C.; Fang, Q.; Chen, D.; Liu, J.; Jiang, X.; Zhang, Y.; Shen, W.; et al. Isoquercitrin Alleviates Diabetic Nephropathy by Inhibiting STAT3 Phosphorylation and Dimerization. *Adv. Sci.* **2025**, *12*, e2414587. [CrossRef] [PubMed]
47. Chen, Y.; Zhang, M.; Jia, R.; Qian, B.; Jing, C.; Zeng, C.; Zhu, D.; Liu, Z.; Zen, K.; Li, L. Podocyte SIRPalpha reduction in diabetic nephropathy aggravates podocyte injury by promoting pyruvate kinase M2 nuclear translocation. *Redox Biol.* **2024**, *78*, 103439. [CrossRef] [PubMed]
48. Liu, L.; Bai, F.; Song, H.; Xiao, R.; Wang, Y.; Yang, H.; Ren, X.; Li, S.; Gao, L.; Ma, C.; et al. Upregulation of TIPE1 in tubular epithelial cell aggravates diabetic nephropathy by disrupting PHB2 mediated mitophagy. *Redox Biol.* **2022**, *50*, 102260. [CrossRef] [PubMed]
49. Tanglai, W.; Wattanapisit, A.; Watanabe, O.; Jeamjitvibool, T.; Lockwood, M.; Cajita, M. Role of Physical Activity in Reducing Diabetic Kidney Disease Risk in Adults: Data From the National Health and Nutrition Examination Survey, 2017–2018. *Diabetes Metab. Res. Rev.* **2025**, *41*, e70055. [CrossRef] [PubMed]
50. Bohm, M.; Schumacher, H.; Werner, C.; Teo, K.K.; Lonn, E.M.; Mahfoud, F.; Speer, T.; Mancia, G.; Redon, J.; Schmieder, R.E.; et al. Association between exercise frequency with renal and cardiovascular outcomes in diabetic and non-diabetic individuals at high cardiovascular risk. *Cardiovasc. Diabetol.* **2022**, *21*, 12. [CrossRef] [PubMed]
51. Yang, R.; Hou, Q.; Chen, R.; Ma, Z.; Jiang, S.; Liu, Z. Protein UHRF1-mediated dual dysregulation of molecular chaperone GRP78 induces endoplasmic reticulum stress and aggravates diabetic nephropathy. *Kidney Int.* **2025**, *108*, 883–900. [CrossRef] [PubMed]
52. Huang, T.S.; Wu, T.; Wu, Y.D.; Li, X.H.; Tan, J.; Shen, C.H.; Xiong, S.J.; Feng, Z.Q.; Gao, S.F.; Li, H.; et al. Long-term statins administration exacerbates diabetic nephropathy via ectopic fat deposition in diabetic mice. *Nat. Commun.* **2023**, *14*, 390. [CrossRef] [PubMed]
53. Kristensen, J.M.; Kjobsted, R.; Larsen, T.J.; Carl, C.S.; Hingst, J.R.; Onslev, J.; Birk, J.B.; Thorup, A.; Steenberg, D.E.; Knudsen, J.R.; et al. Skeletal muscle from TBC1D4 p.Arg684Ter variant carriers is severely insulin resistant but exhibits normal metabolic responses during exercise. *Nat. Metab.* **2024**, *6*, 2254–2266. [CrossRef] [PubMed]

54. Legaard, G.E.; Lyngbaek, M.P.P.; Almdal, T.P.; Karstoft, K.; Bennetsen, S.L.; Feineis, C.S.; Nielsen, N.S.; Durrer, C.G.; Liebetrau, B.; Nystrup, U.; et al. Effects of different doses of exercise and diet-induced weight loss on beta-cell function in type 2 diabetes (DOSE-EX): A randomized clinical trial. *Nat. Metab.* **2023**, *5*, 880–895. [CrossRef] [PubMed]
55. Lay, A.C.; Tran, V.D.T.; Nair, V.; Betin, V.; Hurcombe, J.A.; Barrington, A.F.; Pope, R.J.; Burdet, F.; Mehl, F.; Kryvokhyzha, D.; et al. Profiling of insulin-resistant kidney models and human biopsies reveals common and cell-type-specific mechanisms underpinning Diabetic Kidney Disease. *Nat. Commun.* **2024**, *15*, 10018. [CrossRef] [PubMed]
56. Zhang, Z.; Zhou, D.; Luan, X.; Wang, X.; Zhu, Z.; Luo, W.; Yang, J.; Tang, S.; Song, Y. Biodegradable Hollow Nanoscavengers Restore Liver Functions to Reverse Insulin Resistance in Type 2 Diabetes. *ACS Nano* **2023**, *17*, 9313–9325. [CrossRef] [PubMed]
57. Barutta, F.; Bellini, S.; Kimura, S.; Hase, K.; Corbetta, B.; Corbelli, A.; Fiordaliso, F.; Bruno, S.; Biancone, L.; Barreca, A.; et al. Protective effect of the tunneling nanotube-TNFAIP2/M-sec system on podocyte autophagy in diabetic nephropathy. *Autophagy* **2023**, *19*, 505–524. [CrossRef] [PubMed]
58. Vartak, T.; Godson, C.; Brennan, E. Therapeutic potential of pro-resolving mediators in diabetic kidney disease. *Adv. Drug Deliv. Rev.* **2021**, *178*, 113965. [CrossRef] [PubMed]
59. Fu, T.; Sun, S.; Wang, Z.; Zhao, F.; Zhen, J.; Ji, X.; Xue, F.; Mu, Q.; Wang, Y.; Liu, Y.; et al. Targeting TFAM K76 acetylation attenuates mitochondrial dysfunction and kidney injury in diabetic kidney disease. *Cardiovasc. Diabetol.* **2026**, *25*, 73. [CrossRef] [PubMed]
60. Liu, M.; Yang, W.; Qu, S.; Zhao, T.; Jiang, S.; Peng, S.; Zhang, M.; Xuan, J.; Liu, Z.; Zen, K. Loss of glomerular aldolase B in diabetic nephropathy promotes renal fibrosis via activating Akt/GSK/beta-catenin axis. *J. Adv. Res.* **2025**, *76*, 207–218. [CrossRef] [PubMed]
61. Samir, S.M.; Hassan, H.M.; Elmowafy, R.; Ebrahim, N.A.; Albadawi, E.A.; Albadrani, M.; Owaydhah, W.H.; Elhadidy, M.G. Adjunctive effects of intermittent fasting and exercise with glibenclamide on diabetic nephropathy in rats: A potential role of the polyol pathway. *Front. Physiol.* **2025**, *16*, 1683271. [CrossRef] [PubMed]
62. Zhang, J.; Cui, K.; Wei, H.; Su, H. Mechanism by which 24-week different-volume high-intensity interval training ameliorates renal fibrosis in naturally aging rats via regulating the TGF-beta1/Smad pathway. *Exp. Gerontol.* **2025**, *212*, 112977. [CrossRef] [PubMed]
63. Ru, Q.; Li, Y.; Zhang, X.; Chen, L.; Wu, Y.; Min, J.; Wang, F. Iron homeostasis and ferroptosis in muscle diseases and disorders: Mechanisms and therapeutic prospects. *Bone Res.* **2025**, *13*, 27. [CrossRef] [PubMed]
64. Kolligundla, L.P.; Sullivan, K.M.; Mukhi, D.; Andrade-Silva, M.; Liu, H.; Guan, Y.; Gu, X.; Wu, J.; Doke, T.; Hirohama, D.; et al. Glutathione-specific gamma-glutamylcyclotransferase 1 (CHAC1) increases kidney disease risk by modulating ferroptosis. *Sci. Transl. Med.* **2025**, *17*, eadn3079. [CrossRef] [PubMed]
65. Wang, H.; Yu, X.; Liu, D.; Qiao, Y.; Huo, J.; Pan, S.; Zhou, L.; Wang, R.; Feng, Q.; Liu, Z. VDR Activation Attenuates Renal Tubular Epithelial Cell Ferroptosis by Regulating Nrf2/HO-1 Signaling Pathway in Diabetic Nephropathy. *Adv. Sci.* **2024**, *11*, e2305563. [CrossRef] [PubMed]
66. Wang, H.; Liu, D.; Zheng, B.; Yang, Y.; Qiao, Y.; Li, S.; Pan, S.; Liu, Y.; Feng, Q.; Liu, Z. Emerging Role of Ferroptosis in Diabetic Kidney Disease: Molecular Mechanisms and Therapeutic Opportunities. *Int. J. Biol. Sci.* **2023**, *19*, 2678–2694. [CrossRef] [PubMed]
67. Jimenez-Rondan, F.R.; Ruggiero, C.H.; Cousins, R.J. Zip14 (Slc39a14) metal transporter dysfunction leads to Akkermansia dysbiosis and inflammation in intestinal epithelium via epigenetic changes. *Gut Microbes* **2026**, *18*, 2684080. [CrossRef] [PubMed]
68. Aierken, Y.; He, H.; Li, R.; Lin, Z.; Xu, T.; Zhang, L.; Wu, Y.; Liu, Y. Inhibition of Slc39a14/Slc39a8 reduce vascular calcification via alleviating iron overload induced ferroptosis in vascular smooth muscle cells. *Cardiovasc. Diabetol.* **2024**, *23*, 186. [CrossRef] [PubMed]
69. Wang, Y.; Li, T.; Wang, Y.; Li, J.; Song, L.; Fu, Y.; Li, W.; Li, L.; Qiu, Y.; Yan, J.; et al. Huanglian muxiang decoction alleviates FTH-mediated ferroptosis in colitis by inhibiting the PI3K-AKT pathway. *Phytomedicine* **2026**, *155*, 158083. [CrossRef] [PubMed]
70. Zhang, Y.J.; Cheng, D.; Yao, W.H.; Li, H.; Zhang, M.B.; Mu, Y.W.; Zhang, X.N.; Song, G.; Zeng, T. Spermidine alleviates ethanol-induced hepatocyte ferroptosis by restoring hepatic iron homeostasis via the gut-liver axis. *Phytomedicine* **2026**, *152*, 157853. [CrossRef] [PubMed]
71. Liu, W.; Zhang, S.; Li, Q.; Wu, Y.; Jia, X.; Feng, W.; Li, Z.; Shi, Y.; Hou, Q.; Ma, J.; et al. Lactate modulates iron metabolism by binding soluble adenylyl cyclase. *Cell Metab.* **2023**, *35*, 1597–1612 e1596. [CrossRef] [PubMed]
72. Chen, J.; Liu, D.; Lei, L.; Liu, T.; Pan, S.; Wang, H.; Liu, Y.; Qiao, Y.; Liu, Z.; Feng, Q. CNPY2 Aggravates Renal Tubular Cell Ferroptosis in Diabetic Nephropathy by Regulating PERK/ATF4/CHAC1 Pathway and MAM Integrity. *Adv. Sci.* **2025**, *12*, e2416441. [CrossRef] [PubMed]
73. Mu, K.; Yang, Y.; An, X.; Zhu, J.; Zhang, J.; Jiang, Y.; Yang, X.; Zhang, J. Proteomic analysis of urinary exosomes reveals ferroptosis-associated proteins are involved in diabetic nephropathy. *Genes Dis.* **2024**, *11*, 101138. [CrossRef] [PubMed]
74. Hong, J.; Li, X.; Hao, Y.; Xu, H.; Yu, L.; Meng, Z.; Zhang, J.; Zhu, M. The PRMT6/STAT1/ACSL1 axis promotes ferroptosis in diabetic nephropathy. *Cell Death Differ.* **2024**, *31*, 1561–1575. [CrossRef] [PubMed]

75. Liu, Z.; Huang, T.; Hong, Y.; Yang, Y.; Chen, W.; Zeng, Q.; Chen, Q.; Yang, Y.; Ying, X.; Zeng, W.; et al. Adaptive Antioxidant Nanomedicines Inhibit Ferroptosis in Renal Tubular Epithelial Cells to Alleviate Diabetic Kidney Disease. *Adv. Sci.* **2025**, *12*, e05168. [CrossRef] [PubMed]
76. Shen, R.; Yu, X.; Shi, C.; Fang, Y.; Dai, C.; Zhou, Y. ACSL4 predicts rapid kidney function decline in patients with diabetic kidney disease. *Front. Endocrinol.* **2025**, *16*, 1499555. [CrossRef] [PubMed]
77. Qiu, S.; Xie, D.; Guo, S.; Wang, Z.; Cai, Y.; Wang, Y.; Yu, X.; Guan, Y.; Zhao, Q.; Yang, Q.; et al. Metformin protects podocytes by inhibiting the MAPK14-SLC7A11-GPX4 axis and dysregulation of fatty acid metabolism. *Diabetologia* **2026**, *69*, 3312–3327. [CrossRef] [PubMed]
78. Tian, C.; Chen, Y.; Huang, J.; Zhao, F.; Tang, X.; Gao, J.; Chen, X.; Yuan, X. Balanophora involucrata alleviates diabetic nephropathy by inhibiting ferroptosis, modulating serum metabolites and gut microbiota. *Phytomedicine* **2026**, *151*, 157773. [CrossRef] [PubMed]
79. Tian, R.; Guo, S.; Chen, S.; Wu, J.; Long, A.; Cheng, R.; Wang, X.; Huang, L.; Li, C.; Mao, W.; et al. Natural products as Nrf2 modulators for ferroptosis inhibition in renal disease therapy: Recent progress and future prospects. *Phytomedicine* **2025**, *136*, 156342. [CrossRef] [PubMed]

Disclaimer/Publisher's Note: The statements, opinions and data contained in all publications are solely those of the individual author(s) and contributor(s) and not of MDPI and/or the editor(s). MDPI and/or the editor(s) disclaim responsibility for any injury to people or property resulting from any ideas, methods, instructions or products referred to in the content.